SIAM J. SCI. COMPUT.
Vol. 33, No. 2, pp. 939–965

HIGH ORDER FINITE DIFFERENCE WENO SCHEMES FOR NONLINEAR DEGENERATE PARABOLIC EQUATIONS*

YUANYUAN LIU†, CHI-WANG SHU‡, AND MENGPING ZHANG†

Abstract. High order accurate weighted essentially nonoscillatory (WENO) schemes are usually designed to solve hyperbolic conservation laws or to discretize the first derivative convection terms in convection dominated partial differential equations. In this paper we discuss a high order WENO finite difference discretization for nonlinear degenerate parabolic equations which may contain discontinuous solutions. A porous medium equation (PME) is used as an example to demonstrate the algorithm structure and performance. By directly approximating the second derivative term using a conservative flux difference, the sixth order and eighth order finite difference WENO schemes are constructed. Numerical examples are provided to demonstrate the accuracy and nonoscillatory performance of these schemes.

Key words. weighted essentially nonoscillatory (WENO) scheme, finite difference scheme, nonlinear degenerate parabolic equation, porous medium equation (PME)

AMS subject classification. 65M06

DOI. 10.1137/100791002

1. Introduction.

Weighted essentially nonoscillatory (WENO) schemes were introduced in the literature to approximate hyperbolic conservation laws and the first derivative convection terms in convection dominated convection diffusion partial differential equations (PDEs). The first WENO scheme was introduced in 1994 by Liu, Osher, and Chan in their pioneering paper [21], in which a third order accurate finite volume WENO scheme in one space dimension was constructed. In 1996, Jiang and Shu [17] provided a general framework for designing arbitrary order accurate finite difference WENO schemes, which are more efficient for multidimensional calculations. Very high order WENO schemes are documented in [4]. All these papers use the WENO reconstruction procedure, which is equivalent to a conservative WENO approximation for the first derivative and is the main relevant WENO procedure for designing both conservative finite volume and conservative finite difference schemes to solve hyperbolic conservation laws.

It was realized later that the WENO procedure can also be used in different contexts, such as WENO interpolation and WENO integration. The WENO interpolation procedure is used, for example, in [31] to transfer information from one domain to another in a high order, nonoscillatory fashion for a multidomain WENO scheme, and in [7] to build a high order Lagrangian type method for solving Hamilton–Jacobi equations. The WENO integration procedure is used, for example, in [9, 10] for the design of high order residual distribution conservative finite difference WENO schemes. In our recent work [22], we have studied the positivity of linear weights for various

*Submitted to the journal's Methods and Algorithms for Scientific Computing section April 2, 2010; accepted for publication (in revised form) February 2, 2011; published electronically April 13, 2011.

http://www.siam.org/journals/sisc/33-2/79100.html

†Department of Mathematics, University of Science and Technology of China, Hefei, Anhui 230026, P.R. China (xiaoliu@mail.ustc.edu.cn, mpzhang@ustc.edu.cn). The research of the third author was supported by NSFC grants 11071234 and 91024025.

‡Division of Applied Mathematics, Brown University, Providence, RI 02912 (shu@dam.brown.edu). This author's research was supported by ARO grant W911NF-08-1-0520 and NSF grant DMS-0809086.

WENO procedures, including reconstruction, interpolation, integration, and approximations to higher order derivatives. For an extensive review on WENO schemes, see [34].

In this paper, we are interested in designing WENO schemes for solving the nonlinear, possibly degenerate, parabolic equations

$$u_t = b(u)_{xx}, \tag{1.1}$$

where $a(u) = b'(u) \geq 0$ and it is possible that $a(u) = 0$ for certain values of u. Such equations appear often in applications. For example, the equation modeling the flow of a gas in a porous medium [26, 3],

$$u_t = (u^m)_{xx}, \tag{1.2}$$

in which m is a constant greater than one, belongs to this class. This equation describes various diffusion processes, such as the flow of an isentropic gas through a porous medium, where u is the density of the gas required to be nonnegative and u^{m-1} is the pressure of the gas. Clearly, the equation degenerates at points where $u = 0$, resulting in the phenomenon of finite speed of propagation and sharp fronts.

The classical solutions to the porous medium equation (PME) may not exist in general, even if the initial solution is smooth. Therefore, weak solutions must be considered, and their existence and uniqueness are studied in [1, 12, 29]. The famous Barenblatt solution of the PME (1.2) is a weak solution, found in 1950 by Zel'dovich and Kompaneetz [36] (see also Barenblatt [5]), which is defined explicitly by

$$B_m(x,t) = t^{-k}\left[\left(1 - \frac{k(m-1)}{2m}\frac{|x|^2}{t^{2k}}\right)_+\right]^{1/(m-1)}, \qquad m > 1, \tag{1.3}$$

where $u_+ = \max(u, 0)$ and $k = (m+1)^{-1}$. This solution, for any time $t > 0$, has a compact support $[-\alpha_m(t), \alpha_m(t)]$ with the interface $|x| = \alpha_m(t)$ moving outward at a finite speed, where

$$\alpha_m(t) = \sqrt{\frac{2m}{k(m-1)}}\, t^k.$$

The Barenblatt solution shows that solutions to the PME may have the following properties:

1. Finite speed of propagation: If the initial function has compact support, then at all times the solution $u(\cdot, t)$ will have compact support.
2. Free boundaries: The interface behaves like a free boundary propagating with finite speed.
3. Weak solutions: There exists no derivative at the interface points [23].

Various schemes for approximating (1.1) have been developed in the literature. Linear approximation schemes based on the nonlinear Chernoff formula with a suitable relaxation parameter have been studied in, e.g., [6, 27, 28, 24], where energy error estimates have also been investigated. See also [16, 18] for other types of linear approximation schemes. More recently, a different approach based on kinetic schemes for degenerate parabolic systems has been considered in [2]. Other approaches include that in [13], which is based on a suitable splitting technique with applications to more general hyperbolic-parabolic convection-diffusion equations, and that in [30], which is

based on the maximum principle and on perturbation and regularization. A high order relaxation scheme has been presented in [8]. Finally, a local discontinuous Galerkin finite element method has been constructed in [37] for the PME.

The degenerate parabolic equation (1.1) has features similar to those of a hyperbolic conservation law, such as the possible existence of sharp fronts and finite speed of propagation of wave fronts. Therefore, it is reasonable to generalize numerical techniques for solving hyperbolic conservation laws, such as the WENO technique, to solve (1.1). This would involve a careful adaptation of the WENO procedure to ensure conservation, accuracy, and nonoscillatory performance. In this paper we discuss two different formulations of WENO schemes for approximating (1.1). In section 2, we directly approximate the second derivative term using a conservative flux difference. This approach involves a narrow stencil for a given order of accuracy; however, it would necessarily also involve the usage of negative linear weights, therefore requiring a special treatment such as that in [32] to ensure nonoscillatory performance of the resulting WENO scheme. Numerical examples demonstrating the accuracy and nonoscillatory performance of the sixth order and eighth order WENO schemes are provided. At the end of section 2, we mention briefly the second formulation, which starts with the introduction of an auxiliary variable for the first derivative and then applies the WENO procedure to two first derivatives rather than to the second derivative term directly. This resembles the approach of the local discontinuous Galerkin method [11]. This approach requires only WENO approximations to first derivatives, which is a relatively mature procedure and avoids the appearance of negative linear weights. However, the computational cost is larger since two WENO approximations rather than one must be used to approximate the second derivative. The effective stencil, which is a composition of two successive WENO procedures, is also wider in comparison with the first approach. In section 3, we give brief concluding remarks.

2. Direct WENO discretization to the second derivative. In this section we study a direct WENO discretization to the second derivative in conservation form. Assume that we have a mesh $\cdots < x_1 < x_2 < x_3 < \cdots$, and for simplicity we assume the grid is uniform, i.e., $\Delta x = x_{i+1} - x_i$ is constant. We are building a conservative finite difference scheme for (1.1), written in the form

$$\frac{du_i(t)}{dt} = \frac{\hat{f}_{i+\frac{1}{2}} - \hat{f}_{i-\frac{1}{2}}}{\Delta x^2}, \tag{2.1}$$

where $u_i(t)$ is the numerical approximation to the point value $u(x_i, t)$ of the solution to (1.1), and the numerical flux function

$$\hat{f}_{i+\frac{1}{2}} = \hat{f}(u_{i-r}, \ldots, u_{i+s}) \tag{2.2}$$

is chosen so that the conservative difference on the right-hand side of the scheme (2.1) approximates the second order derivative $(b(u))_{xx}$ at $x = x_i$ to high order accuracy

$$\frac{\hat{f}_{i+\frac{1}{2}} - \hat{f}_{i-\frac{1}{2}}}{\Delta x^2} = (b(u))_{xx}|_{x=x_i} + O(\Delta x^k) \tag{2.3}$$

when the solution is smooth, and it generates nonoscillatory solutions when the solution contains possible discontinuities. We remark that similar schemes for smooth, nonuniform meshes can be designed along the same lines, similar to the conservation case; however, conservative higher than second order approximations on arbitrary

nonsmooth meshes are not possible [25]. The collection of grid points involved in the numerical flux (2.2), $S = \{x_{i-r}, \ldots, x_{i+s}\}$, is called the *stencil* of the flux approximation. A linear scheme is a scheme for which the numerical flux (2.2) is a linear combination of the grid values in the stencil

$$\hat{f}_{i+\frac{1}{2}} = \sum_{j=-r}^{s} a_j b(u_{i+j}), \tag{2.4}$$

where the constant coefficients a_j can be chosen to yield the highest order of accuracy k in (2.3). For example, the classical second order scheme

$$\frac{du_i(t)}{dt} = \frac{b(u_{i+1}) - 2b(u_i) + b(u_{i-1})}{\Delta x^2} \tag{2.5}$$

corresponds to the numerical flux with the stencil $S = \{x_i, x_{i+1}\}$ and is given by

$$\hat{f}_{i+\frac{1}{2}} = -b(u_i) + b(u_{i+1}).$$

The construction of WENO schemes in this section consists of the following steps.

1. We choose a symmetric *big stencil*, $S = \{x_{i-r}, \ldots, x_{i+r+1}\}$, for the numerical flux (2.4), resulting in a linear scheme with an order of accuracy $k = 2r + 2$ in (2.3). This linear scheme should be stable with the designed high order accuracy for smooth solutions but will be oscillatory near discontinuities.
2. We choose s consecutive *small stencils*, $S^m = \{x_{i-r+m}, \ldots, x_{i+r+m+2-s}\}$, for $m = 0, \ldots, s-1$, resulting in a series of lower order linear schemes with their numerical fluxes denoted by $\hat{f}^{(m)}_{i+\frac{1}{2}}$. Here, s can be chosen to be between 2 and $2r+1$, corresponding to each small stencil containing $2r+1$ to 2 points, respectively.
3. We find the *linear weights*, namely, constants d_m, such that the flux on the big stencil is a linear combination of the fluxes on the small stencils with d_m as the combination coefficients

$$\hat{f}_{i+\frac{1}{2}} = \sum_{m=0}^{s-1} d_m \hat{f}^{(m)}_{i+\frac{1}{2}}. \tag{2.6}$$

   If we simply use the linear weights and linear combination on the right-hand side of (2.6), then we would get back the linear scheme on the big stencil, which will be accurate for smooth solutions but will be oscillatory near discontinuities.
4. We change the linear weights d_m in (2.6) to nonlinear weights ω_m, with the objective of maintaining the same high order accuracy for smooth solutions and nonoscillatory performance near discontinuities. This is usually achieved through *smoothness indicators* which measure the smoothness of the function based on different small stencils.

If the linear weights d_m obtained in the third step above are nonnegative, then the linear combination in (2.6) is a convex combination, since by consistency $\sum_{m=0}^{s-1} d_m = 1$. This will help significantly in the design of nonlinear weights in the fourth step above. In [22], we studied the positivity of linear weights for various WENO procedures. However, the current conservative approximation to the second derivative is not considered in [22]. We will therefore start with a discussion on the positivity of the linear weights below, with the rather disappointing conclusion that negative linear weights must appear.

TABLE 2.1
Linear weights in (2.6). *"—" represents the situation in which linear weights do not exist.*

Number of nodes in the big stencil	Number of nodes in each small stencil	Linear weights
4	2	$d_0 = -\frac{1}{12},\ d_1 = \frac{7}{6},\ d_2 = -\frac{1}{12}$
	3	——
6	2	$d_0 = \frac{1}{90},\ d_1 = -\frac{23}{180},\ d_2 = \frac{37}{30},$ $d_3 = -\frac{23}{180},\ d_4 = \frac{1}{90}$
	3	——
	4	$d_0 = -\frac{2}{15},\ d_1 = \frac{19}{15},\ d_2 = -\frac{2}{15}$
	5	——
8	2	$d_0 = -\frac{1}{560},\ d_1 = \frac{11}{504},\ d_2 = -\frac{779}{5040},$ $d_3 = \frac{533}{420},\ d_4 = -\frac{779}{5040},\ d_5 = \frac{11}{504},$ $d_6 = -\frac{1}{560}$
	3	——
	4	$d_0 = -\frac{3}{1540}, d_1 = -\frac{226}{1155},\ d_2 = \frac{293}{210},$ $d_3 = -\frac{226}{1155},\ d_4 = -\frac{3}{1540}$
	5	——
	6	$d_0 = -\frac{9}{56},\ d_1 = \frac{37}{28},\ d_2 = -\frac{9}{56}$
	7	——

2.1. Analysis of the linear weights. In this subsection we study the linear weights d_m in (2.6). In particular, we conclude that it is not possible to maintain all of them as nonnegative. We consider the cases of $r = 1$, 2, and 3, namely, the big stencil containing 4, 6, and 8 points, corresponding to central schemes of fourth, sixth, and eighth order accuracy, respectively.

The linear weights in (2.6), for various numbers of small stencils, are listed in Table 2.1. We conclude from this table that in some cases the linear weights do not exist for (2.6) to hold, and when they do exist, at least one of them is negative.

To explain the nonexistence of linear weights for the cases of odd numbers of nodes in small stencils in Table 2.1, we refer the reader to [22] for a detailed study on the existence and nonexistence of linear weights for various situations. Except for special situations, for example, a WENO interpolation which has linear weights as polynomials themselves, the linear weights for most other cases are rational functions; hence they may not exist at the poles of these functions.

In what follows we will give the details on how to construct the numerical fluxes and obtain the linear weights in section 2.2.

2.2. Direct discretization on the big stencil with six uniform nodes. Now we consider the numerical flux $\hat{f}_{i+\frac{1}{2}}$ on the big stencil with six uniform nodes, that is, $S = \{x_{i-2}, \ldots, x_{i+3}\}$, which corresponds to a sixth order discretization. According to Table 2.1, we can choose either five small stencils each with two nodes, or three small stencils each with four nodes. However, the former would give very low order approximations in each small stencil, thus making the requirement on nonlinear weights very stringent in order to recover sixth order accuracy on the large stencil. This point can be seen in the derivation below. We therefore consider the latter with three small stencils each containing four nodes, that is, $S^m = \{x_{i-2+m}, \ldots, x_{i+1+m}\}$ with $m = 0, 1, 2$.

If we can find a function $h(x)$, which may depend on the grid size Δx, such that

$$b(u(x)) = \frac{1}{\Delta x^2}\int_{x-\frac{\Delta x}{2}}^{x+\frac{\Delta x}{2}}\left(\int_{\eta-\frac{\Delta x}{2}}^{\eta+\frac{\Delta x}{2}} h(\xi)d\xi\right)d\eta, \tag{2.7}$$

then clearly

$$(b(u))_{xx} = \frac{h(x+\Delta x) - 2h(x) + h(x-\Delta x)}{\Delta x^2}. \tag{2.8}$$

If we take the function

$$g(x) = h\left(x + \frac{\Delta x}{2}\right) - h\left(x - \frac{\Delta x}{2}\right), \tag{2.9}$$

we have

$$(b(u))_{xx}|_{x=x_i} = \frac{g(x_{i+\frac{1}{2}}) - g(x_{i-\frac{1}{2}})}{\Delta x^2}, \tag{2.10}$$

which involves no error in approximating the second order spatial derivative with a finite difference.

By approximating $g(x)$ in (2.9), conservative numerical schemes are formulated. These approximations of $g(x)$ are denoted by $p(x)$ and are constructed using a polynomial form with undetermined coefficients. We first consider a polynomial approximation to $h(x)$ of degree at most five on the big stencil S

$$h(x) \approx q(x) = a_0 + a_1 x + a_2 x^2 + a_3 x^3 + a_4 x^4 + a_5 x^5, \tag{2.11}$$

with undetermined coefficients a_k with $k = 0, \ldots, 5$. Substituting (2.11) into (2.7) and performing the integration gives

$$\begin{aligned} b(u(x)) = {} & a_0 + a_1 x + a_2\left(x^2 + \frac{\Delta x^2}{6}\right) + a_3\left(x^3 + \frac{\Delta x^2}{2}x\right) \\ & + a_4\left(x^4 + \Delta x^2 x^2 + \frac{\Delta x^4}{15}\right) + a_5\left(x^5 + \frac{5\Delta x^2}{3}x^3 + \frac{\Delta x^4}{3}x\right). \end{aligned} \tag{2.12}$$

To determine the coefficients $a_0, \ldots, a_5$, one can consider (2.12) as $b(u(-2\Delta x)) = b(u_{i-2}), \ldots, b(u(3\Delta x)) = b(u_{i+3})$ with $x_i = 0$ (the location of x_i is immaterial to the determination of the polynomial coefficients) and solve the resulting system in the unknown coefficients. Therefore, the coefficients a_k can be solved explicitly to yield

$$\begin{aligned} a_0 &= \frac{1}{180}\left(2b(u_{i-2}) - 23b(u_{i-1}) + 222b(u_i) - 23b(u_{i+1}) + 2b(u_{i+2})\right), \\ a_1 &= \frac{1}{120\Delta x}\left(8b(u_{i-2}) - 55b(u_{i-1}) - 70b(u_i) + 160b(u_{i+1}) - 50b(u_{i+2}) + 7b(u_{i+3})\right), \\ a_2 &= \frac{1}{12\Delta x^2}\left(-b(u_{i-2}) + 10b(u_{i-1}) - 18b(u_i) + 10b(u_{i+1}) - b(u_{i+2})\right), \\ a_3 &= \frac{1}{36\Delta x^3}\left(-b(u_{i-2}) - 4b(u_{i-1}) + 20b(u_i) - 26b(u_{i+1}) + 13b(u_{i+2}) - 2b(u_{i+3})\right), \\ a_4 &= \frac{1}{24\Delta x^4}\left(b(u_{i-2}) - 4b(u_{i-1}) + 6b(u_i) - 4b(u_{i+1}) + b(u_{i+2})\right), \\ a_5 &= \frac{1}{120\Delta x^5}\left(-b(u_{i-2}) + 5b(u_{i-1}) - 10b(u_i) + 10b(u_{i+1}) - 5b(u_{i+2}) + b(u_{i+3})\right). \end{aligned}$$

Substituting the coefficients into (2.11) gives the polynomial approximation to $g(x)$ of degree at most four:

$$
\begin{aligned}
&p(x)\\
&= q\left(x+\frac{\Delta x}{2}\right) - q\left(x-\frac{\Delta x}{2}\right)\\
&= \frac{341b(u_{i-2}) - 2785b(u_{i-1}) - 2590b(u_i) + 6670b(u_{i+1}) - 1895b(u_{i+2}) + 259b(u_{i+3})}{5760}\\
&\quad + \left(\frac{-b(u_{i-2}) + 12b(u_{i-1}) - 22b(u_i) + 12b(u_{i+1}) - b(u_{i+2})}{8\Delta x}\right)x\\
&\quad + \left(\frac{-5b(u_{i-2}) - 11b(u_{i-1}) + 70b(u_i) - 94b(u_{i+1}) + 47b(u_{i+2}) - 7b(u_{i+3})}{48\Delta x^2}\right)x^2\\
&\quad + \left(\frac{b(u_{i-2}) - 4b(u_{i-1}) + 6b(u_i) - 4b(u_{i+1}) + b(u_{i+2})}{6\Delta x^3}\right)x^3\\
&\quad + \left(\frac{-b(u_{i-2}) + 5b(u_{i-1}) - 10b(u_i) + 10b(u_{i+1}) - 5b(u_{i+2}) + b(u_{i+3})}{24\Delta x^4}\right)x^4.
\end{aligned}
$$

Evaluating $p(x)$ at $x = x_{i+\frac{1}{2}}$ (recall that $x_i = 0$), we finally obtain the numerical flux on the big stencil

(2.13)
$$
\begin{aligned}
\hat{f}_{i+\frac{1}{2}} &= p(x_{i+\frac{1}{2}})\\
&= \frac{-2b(u_{i-2}) + 25b(u_{i-1}) - 245b(u_i) + 245b(u_{i+1}) - 25b(u_{i+2}) + 2b(u_{i+3})}{180}.
\end{aligned}
$$

We can easily verify that the formula (2.13) does not depend on the location x_i and also that it does not depend on the mesh size Δx; therefore, the numerical flux (2.13) can be used at any interface in the domain. From the definition (2.7) we also know that

$$
\begin{aligned}
\hat{f}_{i+\frac{1}{2}} = \frac{1}{180\Delta x^2}\Bigg(&-2\int_{x_{i-\frac{5}{2}}}^{x_{i-\frac{3}{2}}}\left(\int_{\eta-\frac{\Delta x}{2}}^{\eta+\frac{\Delta x}{2}} h(\xi)d\xi\right)d\eta + 25\int_{x_{i-\frac{3}{2}}}^{x_{i-\frac{1}{2}}}\left(\int_{\eta-\frac{\Delta x}{2}}^{\eta+\frac{\Delta x}{2}} h(\xi)d\xi\right)d\eta\\
&-245\int_{x_{i-\frac{1}{2}}}^{x_{i+\frac{1}{2}}}\left(\int_{\eta-\frac{\Delta x}{2}}^{\eta+\frac{\Delta x}{2}} h(\xi)d\xi\right)d\eta + 245\int_{x_{i+\frac{1}{2}}}^{x_{i+\frac{3}{2}}}\left(\int_{\eta-\frac{\Delta x}{2}}^{\eta+\frac{\Delta x}{2}} h(\xi)d\xi\right)d\eta\\
&-25\int_{x_{i+\frac{3}{2}}}^{x_{i+\frac{5}{2}}}\left(\int_{\eta-\frac{\Delta x}{2}}^{\eta+\frac{\Delta x}{2}} h(\xi)d\xi\right)d\eta + 2\int_{x_{i+\frac{5}{2}}}^{x_{i+\frac{7}{2}}}\left(\int_{\eta-\frac{\Delta x}{2}}^{\eta+\frac{\Delta x}{2}} h(\xi)d\xi\right)d\eta\Bigg).
\end{aligned}
$$

To analyze the accuracy of the approximation to the second derivative for smooth solutions, we assume $h(x)$ has sufficient local regularity. Substituting the Taylor series expansion at the grid point x_i,

$$
h(\xi) = h(x_i) + \sum_{j=1}^{7}\frac{(\xi - x_i)^j}{j!}\frac{d^j h}{dx^j}|_{x=x_i} + O(\Delta x^8),
$$

and performing the integration, we have

$$
\hat{f}_{i+\frac{1}{2}} = \sum_{j=1}^{6}\frac{\Delta x^j}{j!}\frac{d^j h}{dx^j}|_{x=x_i} + \frac{1}{504}\frac{d^7 h}{dx^7}|_{x=x_i}\Delta x^7 + O(\Delta x^8). \tag{2.14}
$$

Comparing (2.14) with the Taylor series expansion

$$g(x_{i+\frac{1}{2}}) = h(x_{i+1}) - h(x_i) = \sum_{j=1}^{6} \frac{\Delta x^j}{j!} \frac{d^j h}{dx^j}|_{x=x_i} + \frac{1}{5040} \frac{d^7 h}{dx^7}|_{x=x_i} \Delta x^7 + O(\Delta x^8), \tag{2.15}$$

we obtain

$$\hat{f}_{i+\frac{1}{2}} = g(x_{i+\frac{1}{2}}) + \frac{1}{560} \frac{d^7 h}{dx^7}|_{x=x_i} \Delta x^7 + O(\Delta x^8). \tag{2.16}$$

Similarly, we calculate the numerical flux $\hat{f}_{i-\frac{1}{2}}$:

$$\begin{aligned} \hat{f}_{i-\frac{1}{2}} &= \frac{-2b(u_{i-3}) + 25b(u_{i-2}) - 245b(u_{i-1}) + 245b(u_i) - 25b(u_{i+1}) + 2b(u_{i+2})}{180} \\ &= g(x_{i-\frac{1}{2}}) + \frac{1}{560} \frac{d^7 h}{dx^7}|_{x=x_i} \Delta x^7 + O(\Delta x^8). \end{aligned} \tag{2.17}$$

Therefore, substituting (2.16) and (2.17) into (2.10), we have the sixth order approximation

$$(b(u))_{xx}|_{x=x_i} = \frac{\hat{f}_{i+\frac{1}{2}} - \hat{f}_{i-\frac{1}{2}}}{\Delta x^2} + O(\Delta x^6). \tag{2.18}$$

Following a similar argument, we obtain a different polynomial of degree at most two, denoted by $p_m(x)$, which approximates the function $g(x)$ in (2.10) on each small stencil $S^m = \{x_{i-2+m}, \ldots, x_{i+1+m}\}$ with $m = 0, 1, 2$:

$$\begin{aligned} p_0(x) &= \frac{5b(u_{i-2}) - 27b(u_{i-1}) + 15b(u_i) + 7b(u_{i+1})}{24} + \left(\frac{b(u_{i-1}) - 2b(u_i) + b(u_{i+1})}{\Delta x} \right) x \\ &\quad + \left(\frac{-b(u_{i-2}) + 3b(u_{i-1}) - 3b(u_i) + b(u_{i+1})}{2\Delta x^2} \right) x^2, \\ p_1(x) &= \frac{-7b(u_{i-1}) - 15b(u_i) + 27b(u_{i+1}) - 5b(u_{i+2})}{24} \\ &\quad + \left(\frac{b(u_{i-1}) - 2b(u_i) + b(u_{i+1})}{\Delta x} \right) x \\ &\quad + \left(\frac{-b(u_{i-1}) + 3b(u_i) - 3b(u_{i+1}) + b(u_{i+2})}{2\Delta x^2} \right) x^2, \\ p_2(x) &= \frac{-43b(u_i) + 69b(u_{i+1}) - 33b(u_{i+2}) + 7b(u_{i+3})}{24} \\ &\quad + \left(\frac{2b(u_i) - 5b(u_{i+1}) + 4b(u_{i+2}) - b(u_{i+3})}{\Delta x} \right) x \\ &\quad + \left(\frac{-b(u_i) + 3b(u_{i+1}) - 3b(u_{i+2}) + b(u_{i+3})}{2\Delta x^2} \right) x^2, \end{aligned} \tag{2.19}$$

where again we assume that $x_i = 0$. The approximations are evaluated at the point $x_{i+\frac{1}{2}}$ to obtain the numerical fluxes on the small stencils $S^m = \{x_{i-2+m}, \ldots, x_{i+1+m}\}$ with $m = 0, 1, 2$:

$$\hat{f}^{(0)}_{i+\frac{1}{2}} = \frac{b(u_{i-2}) - 3b(u_{i-1}) - 9b(u_i) + 11b(u_{i+1})}{12},$$

$$\hat{f}^{(1)}_{i+\frac{1}{2}} = \frac{b(u_{i-1}) - 15b(u_i) + 15b(u_{i+1}) - b(u_{i+2})}{12}, \tag{2.20}$$
$$\hat{f}^{(2)}_{i+\frac{1}{2}} = \frac{-11b(u_i) + 9b(u_{i+1}) + 3b(u_{i+2}) - b(u_{i+3})}{12}.$$

We need only to shift each index by -1 to obtain the flux $\hat{f}^{(m)}_{i-\frac{1}{2}}$. Hence the Taylor series expansions of (2.20) give

$$\hat{f}^{(0)}_{i\pm\frac{1}{2}} = g(x_{i\pm\frac{1}{2}}) + \frac{1}{12}\frac{d^4h}{dx^4}|_{x=x_i}\Delta x^4 + O(\Delta x^5),$$
$$\hat{f}^{(1)}_{i\pm\frac{1}{2}} = g(x_{i\pm\frac{1}{2}}) - \frac{1}{90}\frac{d^5h}{dx^5}|_{x=x_i}\Delta x^5 + O(\Delta x^6), \tag{2.21}$$
$$\hat{f}^{(2)}_{i\pm\frac{1}{2}} = g(x_{i\pm\frac{1}{2}}) - \frac{1}{12}\frac{d^4h}{dx^4}|_{x=x_i}\Delta x^4 + O(\Delta x^5)$$

and the finite difference approximations

$$(b(u))_{xx}|_{x=x_i} = \frac{\hat{f}^{(0)}_{i+\frac{1}{2}} - \hat{f}^{(0)}_{i-\frac{1}{2}}}{\Delta x^2} + O(\Delta x^3),$$
$$(b(u))_{xx}|_{x=x_i} = \frac{\hat{f}^{(1)}_{i+\frac{1}{2}} - \hat{f}^{(1)}_{i-\frac{1}{2}}}{\Delta x^2} + O(\Delta x^4), \tag{2.22}$$
$$(b(u))_{xx}|_{x=x_i} = \frac{\hat{f}^{(2)}_{i+\frac{1}{2}} - \hat{f}^{(2)}_{i-\frac{1}{2}}}{\Delta x^2} + O(\Delta x^3).$$

We also obtain the linear weights

$$d_0 = -\frac{2}{15}, \qquad d_1 = \frac{19}{15}, \qquad d_2 = -\frac{2}{15} \tag{2.23}$$

satisfying

$$\hat{f}_{i+\frac{1}{2}} = \sum_{m=0}^{2} d_m \, \hat{f}^{(m)}_{i+\frac{1}{2}},$$

where $\hat{f}_{i+\frac{1}{2}}$ and $\hat{f}^{(m)}_{i+\frac{1}{2}}$ are given in (2.13) and (2.20), respectively.

2.2.1. A technique of treating negative weights. Notice that the linear weights d_0 and d_2 are negative. WENO procedures cannot be applied directly to obtain a stable scheme if negative linear weights are present. Test cases for both scalar equations and systems were shown in [32], indicating that the presence of negative weights without special treatment may lead to instability (blow-up of the numerical solution) of WENO schemes. We use the technique in [32] to treat the negative weights in (2.23). We split the linear weights into two parts, positive and negative, by defining

$$\tilde{\gamma}^+_m = \frac{1}{2}(d_m + \theta|d_m|), \quad \tilde{\gamma}^-_m = \tilde{\gamma}^+_m - d_m, \quad m = 0, 1, 2,$$

where $\theta = 3$. Then we obtain

$$\tilde{\gamma}^+_0 = \frac{2}{15}, \qquad \tilde{\gamma}^+_1 = \frac{38}{15}, \qquad \tilde{\gamma}^+_2 = \frac{2}{15};$$

$$\tilde{\gamma}_0^- = \frac{4}{15}, \qquad \tilde{\gamma}_1^- = \frac{19}{15}, \qquad \tilde{\gamma}_2^- = \frac{4}{15}.$$

We scale them by

$$\sigma^+ = \sum_{m=0}^{2} \tilde{\gamma}_m^+ = \frac{42}{15}, \quad \sigma^- = \sum_{m=0}^{2} \tilde{\gamma}_m^- = \frac{27}{15} \tag{2.24}$$

and obtain the linear weights of the two parts by $\gamma_m^\pm = \tilde{\gamma}_m^\pm/\sigma^\pm$ with $m = 0, 1, 2$:

$$\gamma_0^+ = \frac{1}{21}, \qquad \gamma_1^+ = \frac{19}{21}, \qquad \gamma_2^+ = \frac{1}{21}; \tag{2.25}$$

$$\gamma_0^- = \frac{4}{27}, \qquad \gamma_1^- = \frac{19}{27}, \qquad \gamma_2^- = \frac{4}{27}. \tag{2.26}$$

It is easy to check that

$$\sum_{m=0}^{2} \gamma_m^\pm = 1 \quad \text{and} \quad d_m = \sigma^+\gamma_m^+ - \sigma^-\gamma_m^-. \tag{2.27}$$

2.2.2. The smoothness indicators and the nonlinear weights. To change the linear weights to nonlinear weights, we use the definition of the smoothness function in [17, 33],

$$\beta_m = \sum_{l=1}^{\tilde{k}} \Delta x^{2l-1} \int_{x_i}^{x_{i+1}} \left(\frac{d^l}{dx^l} p_m(x)\right)^2 dx, \tag{2.28}$$

where the approximation polynomials $p_m(x)$ on the small stencils $S^m = \{x_{i-2+m}, \ldots, x_{i+1+m}\}$ with $m = 0, 1, 2$ are given in (2.19) and $\tilde{k}$ is the degree of $p_m(x)$ (here $\tilde{k} = 2$), and obtain the smoothness indicators

$$\begin{aligned}
\beta_0 &= \frac{13}{12}(b(u_{i-2}) - 3b(u_{i-1}) + 3b(u_i) - b(u_{i+1}))^2 \\
&\quad + \frac{1}{4}(b(u_{i-2}) - 5b(u_{i-1}) + 7b(u_i) - 3b(u_{i+1}))^2, \\
\beta_1 &= \frac{13}{12}(b(u_{i-1}) - 3b(u_i) + 3b(u_{i+1}) - b(u_{i+2}))^2 \\
&\quad + \frac{1}{4}(b(u_{i-1}) - b(u_i) - b(u_{i+1}) + b(u_{i+2}))^2, \\
\beta_2 &= \frac{13}{12}(b(u_i) - 3b(u_{i+1}) + 3b(u_{i+2}) - b(u_{i+3}))^2 \\
&\quad + \frac{1}{4}(-3b(u_i) + 7b(u_{i+1}) - 5b(u_{i+2}) + b(u_{i+3}))^2.
\end{aligned} \tag{2.29}$$

Here we perform the integration over the interval $[x_i, x_{i+1}]$ to satisfy the symmetry property of the parabolic equation, and the factor Δx^{2l-1} in (2.28) is introduced to remove any Δx dependency in the final expression of the smoothness indicators in (2.29).

For the positive and negative linear weights $\gamma_m^\pm$ in (2.25) and (2.26), we define the nonlinear weights for the positive and negative groups $\tilde{\omega}_m^\pm$, respectively, denoted by $\omega_m^\pm$, based on the same smoothness indicators β_m given in (2.29),

$$\omega_m^\pm = \frac{\tilde{\omega}_m^\pm}{\sum_{l=0}^{2} \tilde{\omega}_l^\pm}, \qquad \tilde{\omega}_m^\pm = \frac{\gamma_m^\pm}{(\epsilon + \beta_m)^2}, \qquad m = 0, 1, 2, \tag{2.30}$$

where ϵ prevents the denominator from becoming zero. In this paper we take $\epsilon = 10^{-6}$ unless otherwise stated. It is easy to verify that $\sum_{m=0}^{2} \omega_m^{\pm} = 1$.

2.2.3. The finite difference WENO scheme. Rewriting the positive and negative nonlinear weights in (2.30) together, we finally obtain the nonlinear weights

$$\omega_m = \sigma^+ \omega_m^+ - \sigma^- \omega_m^-, \tag{2.31}$$

with $\sigma^{\pm}$ given in (2.24), and the WENO approximation flux

$$\hat{f}_{i+\frac{1}{2}} = \sum_{m=0}^{2} \omega_m \hat{f}_{i+\frac{1}{2}}^{(m)}, \tag{2.32}$$

where $\hat{f}_{i+\frac{1}{2}}^{(m)}$ with $m = 0, 1, 2$ are given by (2.20).

Then the semidiscrete finite difference WENO scheme can be expressed as

$$\frac{du_i(t)}{dt} = \frac{\hat{f}_{i+\frac{1}{2}} - \hat{f}_{i-\frac{1}{2}}}{\Delta x^2}. \tag{2.33}$$

2.2.4. Runge–Kutta time discretization. Up until now we have considered only spatial discretization, leaving the time variable continuous. After the spatial discretization, the semidiscrete finite difference WENO scheme is equivalent to the first order ODE system

$$\frac{du(t)}{dt} = L(u), \tag{2.34}$$

where $L(u)$ results from the right-hand side of (2.33). This ODE system can then be discretized by a suitable ODE solver.

For the sixth order WENO scheme, we use the third order total variation diminishing (TVD) Runge–Kutta method [35] to solve (2.34), which is given by

$$\begin{aligned} u^{(1)} &= u^n + \Delta t L(u^n), \\ u^{(2)} &= \frac{3}{4}u^n + \frac{1}{4}u^{(1)} + \frac{1}{4}\Delta t L(u^{(1)}), \\ u^{n+1} &= \frac{1}{3}u^n + \frac{2}{3}u^{(2)} + \frac{2}{3}\Delta t L(u^{(2)}). \end{aligned}$$

This explicit time discretization has the advantage of maintaining nonlinear stability; however, it may not be the most efficient solver because of the time step restriction $\Delta t = O(\Delta x^2)$. Nevertheless, for convection dominated convection-diffusion equations this time discretization could still be a suitable choice, because the diffusion coefficient in front of the $O(\Delta x^2)$ term in the stability condition is relatively small.

2.3. Analysis of the accuracy of the finite difference WENO scheme. In order to achieve the objective of maintaining the same high order accuracy as in (2.18) in smooth regions and nonoscillatory performance in regions where a discontinuity does exist, we need to find out the accuracy requirement of the finite difference WENO scheme (2.33).

Adding and subtracting $\sum_{m=0}^{2} d_m \hat{f}_{i+\frac{1}{2}}^{(m)}$ from (2.32) gives

$$\hat{f}_{i+\frac{1}{2}} = \underbrace{\sum_{m=0}^{2} d_m \hat{f}_{i+\frac{1}{2}}^{(m)}}_{g(x_{i+\frac{1}{2}}) + \frac{1}{560}\frac{d^7 h}{dx^7}|_{x=x_i}\Delta x^7 + O(\Delta x^8)} + \sum_{m=0}^{2} (\omega_m - d_m)\hat{f}_{i+\frac{1}{2}}^{(m)}, \tag{2.35}$$

where the second term must be at least $O(\Delta x^7)$ if it is smooth, or $O(\Delta x^8)$ if it is discontinuous, in order to guarantee the approximation to the second order derivative to be sixth order accurate.

Substituting the numerical fluxes $\hat{f}^{(m)}_{i+\frac{1}{2}}$ given in (2.21) and expanding the second term, we obtain

$$\begin{aligned}
&\sum_{m=0}^{2}(\omega_m - d_m)\hat{f}^{(m)}_{i+\frac{1}{2}} \\
&= (\omega_0 - d_0)\left(g(x_{i+\frac{1}{2}}) + \frac{1}{12}\frac{d^4h}{dx^4}|_{x=x_i}\Delta x^4 + O(\Delta x^5)\right) \\
&\quad + (\omega_1 - d_1)\left(g(x_{i+\frac{1}{2}}) - \frac{1}{90}\frac{d^5h}{dx^5}|_{x=x_i}\Delta x^5 + O(\Delta x^6)\right) \\
&\quad + (\omega_2 - d_2)\left(g(x_{i+\frac{1}{2}}) - \frac{1}{12}\frac{d^4h}{dx^4}|_{x=x_i}\Delta x^4 + O(\Delta x^5)\right) \\
&= g(x_{i+\frac{1}{2}})\sum_{m=0}^{2}(\omega_m - d_m) + \frac{1}{12}\frac{d^4h}{dx^4}|_{x=x_i}\Delta x^4(\omega_0 - \omega_2) + \sum_{m=0}^{2}(\omega_m - d_m)\Delta x^5. \qquad (2.36)
\end{aligned}$$

Notice that $d_0 = d_2$ and $\sum_{m=0}^{2} d_m = \sum_{m=0}^{2}\omega_m = 1$. Thus we obtain the sufficient conditions to achieve sixth order accuracy convergence

$$\omega_0 - \omega_2 = O(\Delta x^4), \qquad (2.37)$$

$$\omega_m - d_m = O(\Delta x^3). \qquad (2.38)$$

Equation (2.38) gives us a simple set of criteria around which to design the nonlinear weights ω_m, while (2.37) is a difficult constraint to use in the design of the nonlinear weights.

Therefore, in order to satisfy conditions (2.37) and (2.38), we have to analyze the nonlinear weights from (2.31). First, we will consider the smoothness indicators β_m with $m = 0, 1, 2$.

2.3.1. The analysis of the smoothness indicators. We expand the smoothness indicators β_m (2.29) with $m = 0, 1, 2$ at the grid point x_i:

$$\begin{aligned}
\beta_0 &= b_{xx}^2\Delta x^4 + b_{xx}b_{xxx}\Delta x^5 + \frac{1}{3}(4b_{xxx}^2 - b_{xx}b_{xxxx})\Delta x^6 + O(\Delta x^7), \\
\beta_1 &= b_{xx}^2\Delta x^4 + b_{xx}b_{xxx}\Delta x^5 + \frac{2}{3}(2b_{xxx}^2 + b_{xx}b_{xxxx})\Delta x^6 + O(\Delta x^7), \\
\beta_2 &= b_{xx}^2\Delta x^4 + b_{xx}b_{xxx}\Delta x^5 + \frac{1}{3}(4b_{xxx}^2 - b_{xx}b_{xxxx})\Delta x^6 + O(\Delta x^7).
\end{aligned}$$

Therefore, if

1. $b_{xx} \neq 0$, we have $\beta_m = D(1 + O(\Delta x))$ with $m = 0, 1, 2$, and if
2. $b_{xx} = 0, b_{xxx} \neq 0$, we have $\beta_m = D(1 + O(\Delta x))$ with $m = 0, 1, 2$,

where D is a nonzero quantity independent of m (but may depend on the derivatives of $b(u(x))$ and Δx). From the previous analysis we have

$$\beta_m = D(1 + O(\Delta x)), \qquad m = 0, 1, 2. \qquad (2.39)$$

2.3.2. The relationship among β_m, γ_m, and ω_m. Through a Taylor expansion analysis, we conclude that $\beta_m = D(1 + O(\Delta x^{k-1}))$ is the sufficient condition so that $\omega_m = d_m + O(\Delta x^{k-1})$ holds, where D is a nonzero quantity independent of m (but may depend on Δx).

Because of the Taylor expansion $\frac{1}{(1+x)^2} = 1 - 2x + 3x^2 \cdots$ near $x = 0$, and neglecting ϵ, we obtain

$$\frac{\gamma_m^{\pm}}{(\epsilon+\beta_m)^2} = \frac{\gamma_m^{\pm}}{(D(1+O(\Delta x^{k-1})))^2} = \frac{\gamma_m^{\pm}}{D^2}(1 + O(\Delta x^{k-1})).$$

From the definition of the nonlinear weights in (2.30) and $\sum_{m=0}^{2} \gamma_m^{\pm} = 1$, we have

$$\begin{aligned}\gamma_m^{\pm} &= \omega_m^{\pm}\left(\sum_{l=0}^{2}\frac{\gamma_l^{\pm}}{(\epsilon+\beta_l)^2}\right)(\epsilon+\beta_m)^2 \\ &= \omega_m^{\pm}\left(\frac{1}{D^2}(1+O(\Delta x^{k-1}))\right)(D(1+O(\Delta x^{k-1})))^2 \\ &= \omega_m^{\pm} + O(\Delta x^{k-1}), \qquad m = 0,1,2. \end{aligned} \tag{2.40}$$

Thus, through the previous analysis, the conditions (2.27), (2.39), and (2.40) imply that the nonlinear weights defined in (2.30) and (2.31) are given by

$$\omega_m = d_m + O(\Delta x), \qquad m = 0,1,2. \tag{2.41}$$

Unfortunately, in this case the condition (2.38) is not satisfied; that is, we cannot achieve sixth order accuracy by using only the nonlinear weights defined in (2.30) and (2.31).

2.3.3. Mapped nonlinear weights. To increase the accuracy of the nonlinear weights, we use the mapped function introduced in [15]:

$$\mathrm{g}_m(\omega) = \frac{\omega(d_m + d_m^2 - 3d_m\omega + \omega^2)}{d_m^2 + \omega(1-2d_m)}, \quad m = 0,1,2. \tag{2.42}$$

This function is monotonically increasing with a finite slope, $\mathrm{g}_m(0) = 0$, $\mathrm{g}_m(1) = 1$, $\mathrm{g}_m(d_m) = d_m$, $\mathrm{g}_m^{'}(d_m) = 0$, and $\mathrm{g}_m^{''}(d_m) = 0$. The mapped nonlinear weights are given by

$$\alpha_m = \mathrm{g}_m(\omega_m), \qquad m = 0,1,2, \tag{2.43}$$

where d_m and ω_m are computed in (2.23), (2.30), and (2.31), respectively.

The mapped nonlinear weights are then defined as

$$\omega_m^{(M)} = \frac{\alpha_m}{\sum_{m=0}^{2}\alpha_m}, \qquad m = 0,1,2. \tag{2.44}$$

Hence the final form of the semidiscrete finite difference mapped WENO scheme is

$$\frac{du_i(t)}{dt} = \frac{\hat{f}_{i+\frac{1}{2}} - \hat{f}_{i-\frac{1}{2}}}{\Delta x^2}, \tag{2.45}$$

with the approximation flux

$$\hat{f}_{i+\frac{1}{2}} = \sum_{m=0}^{2}\omega_m^{(M)}\hat{f}_{i+\frac{1}{2}}^{(m)}, \tag{2.46}$$

where $\hat{f}_{i+\frac{1}{2}}^{(m)}$ with $m = 0, 1, 2$ are given by (2.20).

By Taylor series approximation of the $\mathrm{g}_m(\omega)$ at d_m and the condition (2.41) we have

$$\begin{aligned}\alpha_m &= \mathrm{g}_m(d_m) + \mathrm{g}_m^{'}(d_m)(\omega_m - d_m) \\ &\quad + \frac{\mathrm{g}_m^{''}(d_m)}{2}(\omega_m - d_m)^2 + \frac{\mathrm{g}_m^{'''}(d_m)}{6}(\omega_m - d_m)^3 + \cdots \\ &= d_m + \frac{(\omega_m - d_m)^3}{d_m - d_m^2} + \frac{\mathrm{g}_m^{''''}(d_m)}{24}(\omega_m - d_m)^4 + \cdots \\ &= d_m + O(\Delta x^3) + \frac{\mathrm{g}_m^{''''}(d_m)}{24}O(\Delta x^4),\end{aligned} \tag{2.47}$$

and then

$$\begin{aligned}\omega_m^{(M)} &= \left(d_m + O(\Delta x^3) + \frac{\mathrm{g}_m^{''''}(d_m)}{24}O(\Delta x^4)\right)(1 + O(\Delta x^3)) \\ &= d_m + O(\Delta x^3) + \frac{\mathrm{g}_m^{''''}(d_m)}{24}O(\Delta x^4),\end{aligned} \tag{2.48}$$

$$\omega_0^{(M)} - \omega_2^{(M)} = O(\Delta x^4) \tag{2.49}$$

because of $\sum_{m=0}^{2} d_m = 1$ and $d_0 = d_2$. Now conditions (2.37) and (2.38) are satisfied; therefore, the mapped WENO scheme (2.45) has sixth order accuracy for smooth solutions and is nonoscillatory near discontinuities, as verified by numerical experiments given later.

Given the grid point values of $b(u)$, the algorithm flowchart of our sixth order finite difference WENO scheme with the third order TVD Runge–Kutta method in time for the nonlinear degenerate parabolic equation (1.1) is as follows:

- Evaluate the numerical fluxes $\hat{f}_{i+\frac{1}{2}}^{(m)}$ by (2.20) and the smoothness indicators β_m by (2.29).
- Split the negative linear weights d_m (2.23) into positive and negative parts $\gamma_m^{\pm}$ by (2.25) and (2.26).
- Define the nonlinear weights for the positive and negative groups $\omega_m^{\pm}$ (2.30) to compute the nonlinear weights ω_m (2.31).
- Apply the mapped function $\mathrm{g}_m(\omega)$ by (2.42) and (2.43) to obtain the final nonlinear weights $\omega_m^{(M)}$ (2.44) and the numerical flux $\hat{f}_{i+\frac{1}{2}}$ by (2.46) in the semidiscrete finite difference WENO scheme (2.45).
- Use the third order TVD Runge–Kutta method for time discretization.

The time-step must be selected to satisfy a Courant–Friedrichs–Lewy (CFL) stability condition to ensure numerical stability. In order to determine the CFL condition of the form $\Delta t \le C\Delta x^2$, we consider the linear case, that is, the sixth order finite difference scheme with the third order TVD Runge–Kutta method in time for the heat equation $u_t = u_{xx}$. Substituting the numerical flux (2.13) into (2.1) and the third order TVD Runge–Kutta method, by Fourier transform we deduce the amplification factor

$$\begin{aligned}Q(\xi) = 1 &+ \sigma\left(-\frac{109}{45} + \frac{44}{15}\cos\xi - \frac{3}{5}\cos^2\xi + \frac{4}{45}\cos^3\xi\right) \\ &+ \sigma^2\left(\frac{11881}{4050} - \frac{4796}{675}\cos\xi + \frac{259}{45}\cos^2\xi - \frac{160}{81}\cos^3\xi + \frac{119}{270}\cos^4\xi\right.\end{aligned}$$

$$-\frac{4}{75}\cos^5\xi+\frac{8}{2025}\cos^6\xi\Big)$$
$$+\sigma^3\Big(-\frac{1295029}{546750}+\frac{261382}{30375}\cos\xi-\frac{246667}{20250}\cos^2\xi+\frac{795566}{91125}\cos^3\xi$$
$$-\frac{221671}{60750}\cos^4\xi+\frac{10526}{10125}\cos^5\xi-\frac{36817}{182250}\cos^6\xi+\frac{838}{30375}\cos^7\xi$$
$$-\frac{8}{3375}\cos^8\xi+\frac{32}{273375}\cos^9\xi\Big).$$

Here $\sigma=\frac{\Delta t}{\Delta x^2}$. From the stability condition $|Q(\xi)|\le 1$ for all $\xi\in[-\pi,\pi]$, we obtain the CFL condition

$$0<\sigma=\frac{\Delta t}{\Delta x^2}\le 0.415712.$$

2.4. Direct discretization on the big stencil with eight uniform nodes. In section 2.1 we considered the linear weights for the cases that the big stencil contains four, six, and eight points, and we have constructed the sixth order finite difference WENO scheme on the big stencil with six uniform nodes. The two remaining cases to consider are the direct discretization to the second derivative on the big stencil containing four and eight uniform nodes, which corresponds to fourth and eighth order discretizations. From the analysis in section 2.2, we observe that when the small stencil contains k uniform nodes, the degree of the approximation polynomial $p_m(x)$ is $k-2$. Therefore, we cannot define the smoothness indicators through the definition (2.28) when the small stencil contains two uniform nodes. Hence, in this section we consider only the big stencil $S=\{x_{i-3},\dots,x_{i+4}\}$ with eight uniform nodes and the small stencil with four and six uniform nodes, respectively.

Following arguments similar to those in section 2.3, when the small stencil contains four uniform nodes, we have the smoothness indicators expressed as $\beta_m=D(1+O(\Delta x))$, the difference between the nonlinear weights and the linear weights being $\omega_m=d_m+O(\Delta x)$, and then $\omega_m^{(M)}=d_m+O(\Delta x^3)$ by applying the mapped function. Unfortunately we need $\omega_m^{(M)}=d_m+O(\Delta x^5)$ to achieve eighth order accuracy of the finite difference WENO schemes on the big stencil with eight uniform nodes, so this choice is not desirable.

Thus we consider the small stencil $S^m=\{x_{i-3+m},\dots,x_{i+2+m}\}$ with six uniform nodes, with the numerical fluxes given by

(2.50)
$$\hat f^{(0)}_{i+\frac12}=\frac{-2b(u_{i-3})+10b(u_{i-2})-5b(u_{i-1})-205b(u_i)+215b(u_{i+1})-13b(u_{i+2})}{180},$$
$$\hat f^{(1)}_{i+\frac12}=\frac{-2b(u_{i-2})+25b(u_{i-1})-245b(u_i)+245b(u_{i+1})-25b(u_{i+2})+2b(u_{i+3})}{180},$$
$$\hat f^{(2)}_{i+\frac12}=\frac{13b(u_{i-1})-215b(u_i)+205b(u_{i+1})+5b(u_{i+2})-10b(u_{i+3})+2b(u_{i+4})}{180}$$

and the linear weights

$$d_0=-\frac{9}{56},\qquad d_1=\frac{37}{28},\qquad d_2=-\frac{9}{56}. \tag{2.51}$$

The degree of the approximation polynomial $p_m(x)$ on each small stencil is four with

$m = 0, 1, 2$, and hence the smoothness indicator β_m on each small stencil S^m is

$$\beta_m = \sum_{l=1}^{4} \Delta x^{2l-1} \int_{x_i}^{x_{i+1}} \left(\frac{d^l}{dx^l} p_m(x) \right)^2 dx \tag{2.52}$$

by the definition (2.28).

For time discretization we use the fourth order Runge–Kutta method

$$\begin{aligned} u^{(1)} &= u^n + \frac{1}{2}\Delta t L(u^n), \\ u^{(2)} &= u^n + \frac{1}{2}\Delta t L(u^{(1)}), \\ u^{(3)} &= u^n + \Delta t L(u^{(2)}), \\ u^{n+1} &= \frac{1}{3}(-u^n + u^{(1)} + 2u^{(2)} + u^{(3)}) + \frac{1}{6}\Delta t L(u^{(3)}). \end{aligned}$$

Although this fourth order Runge–Kutta method is not TVD, it can be made TVD by an increase of operation counts [35]. Finally, we obtain the eighth order finite difference WENO scheme by using an algorithm flowchart similar to that presented in section 2.3.3. We omit the details to save space. Using the Fourier transform, we compute the CFL stability condition for the linear problem

$$0 < \sigma = \frac{\Delta t}{\Delta x^2} \le 0.428402.$$

From an analysis similar to that in section 2.3, we know the finite difference WENO scheme has eighth order accuracy for smooth solutions and is nonoscillatory near discontinuities, as shown in numerical experiments.

2.5. Numerical results.

Example 1. We first test the accuracy of the sixth order and the eighth order finite difference WENO schemes for the case $m = 1$ in (1.2), that is, the linear initial value problem with periodic boundary condition

$$\begin{cases} u_t = u_{xx}, \\ u(x, 0) = \sin(x), \quad -\pi \le x < \pi. \end{cases} \tag{2.53}$$

It is easy to verify that the exact solution of problem (2.53) is

$$u^e(x, t) = e^{-t} \sin(x).$$

The norm of the error is computed by a comparison with the exact solution at the final time according to

$$L^1 = \frac{1}{N+1} \sum_{i=0}^{N} |u_i^n - u^e(x_i, t)|, \tag{2.54}$$

$$L^\infty = \max_{0 \le i \le N} |u_i^n - u^e(x_i, t)|, \tag{2.55}$$

where $u^e(x_i, t)$ denotes the exact solution of the PDE.

In Table 2.2 we show the results of the sixth order WENO scheme (2.45) with $\Delta t = 0.4\Delta x^2$ at the final time $T = 2$. We can clearly see that the designed order of accuracy

TABLE 2.2
Accuracy of sixth WENO on $u_t = u_{xx}$ with $u(x,0) = \sin(x)$.

	$\epsilon = 10^{-6}$				$\epsilon = 10^{-14}$			
N	L^1 error	order	L^∞ error	order	L^1 error	order	L^∞ error	order
10	4.93E-06	–	7.81E-06	–	4.93E-06	–	7.81E-06	–
20	1.35E-07	5.19	2.21E-07	5.14	1.35E-07	5.19	2.21E-07	5.14
40	2.25E-09	5.90	3.63E-09	5.93	2.25E-09	5.91	3.63E-09	5.93
80	3.54E-11	5.99	5.63E-11	6.01	3.54E-11	5.99	5.63E-11	6.01
160	5.68E-13	5.96	8.98E-13	5.97	5.67E-13	5.96	8.97E-13	5.97

is obtained. We use two different values of the parameter ϵ in the nonlinear weights (2.30), observing little difference in the errors, which indicates that the accuracy is not sensitive to the choice of ϵ.

We also present the results of the eighth order WENO scheme (2.45) with $\Delta t = 0.4\Delta x^2$, at the final time $T = 2$, as shown in Table 2.3. Again we observe the designed order of accuracy.

TABLE 2.3
Accuracy of eighth WENO on $u_t = u_{xx}$ with $u(x,0) = \sin(x)$.

	$\epsilon = 10^{-6}$				$\epsilon = 10^{-14}$			
N	L^1 error	order	L^∞ error	order	L^1 error	order	L^∞ error	order
10	1.93E-06	–	3.28E-06	–	1.93E-06	–	3.28E-06	–
20	8.16E-09	7.88	1.36E-08	7.91	8.16E-09	7.88	1.36E-08	7.91
40	3.30E-11	7.95	5.32E-11	8.00	3.30E-11	7.95	5.32E-11	8.00
80	1.26E-13	8.03	2.01E-13	8.05	1.26E-13	8.03	2.00E-13	8.05

Example 2. Then we begin our simulation for the Barenblatt solution given in (1.3) for the PME (1.2), where the initial condition is taken as the Barenblatt solution at $t = 1$, and the boundary condition is $u(\pm 6, t) = 0$ for $t > 1$.

To solve the nonlinear degenerate parabolic equation (1.1), we have the CFL conditions

$$\max_u |b'(u)| \frac{\Delta t}{\Delta x^2} \le 0.415712$$

and

$$\max_u |b'(u)| \frac{\Delta t}{\Delta x^2} \le 0.428402,$$

which should be satisfied for the sixth and eighth order WENO schemes, respectively. Therefore, we choose $\max_u |b'(u)| \frac{\Delta t}{\Delta x^2} = 0.4$ for both schemes. We divide the computational domain into $N = 160$ uniform cells and plot the numerical solution at $T = 2$, respectively, for $m = 2, 3, 5$, and 8. The results are shown in Figure 2.1, in which the circle-box and the square-box are the numerical solutions computed by the sixth and eighth order WENO schemes, respectively, and the solid line is the exact solution.

We observe that the WENO schemes can simulate the Barenblatt solution accurately and sharply, without noticeable oscillations near the interface. There is a slight undershoot for the eighth order scheme near the discontinuity, probably due to the fact that the fourth order Runge–Kutta method is not TVD. We have verified that this undershoot disappears when we take a smaller time-step, indicating that it is related to the time discretization rather than the spatial operator. Likewise, both

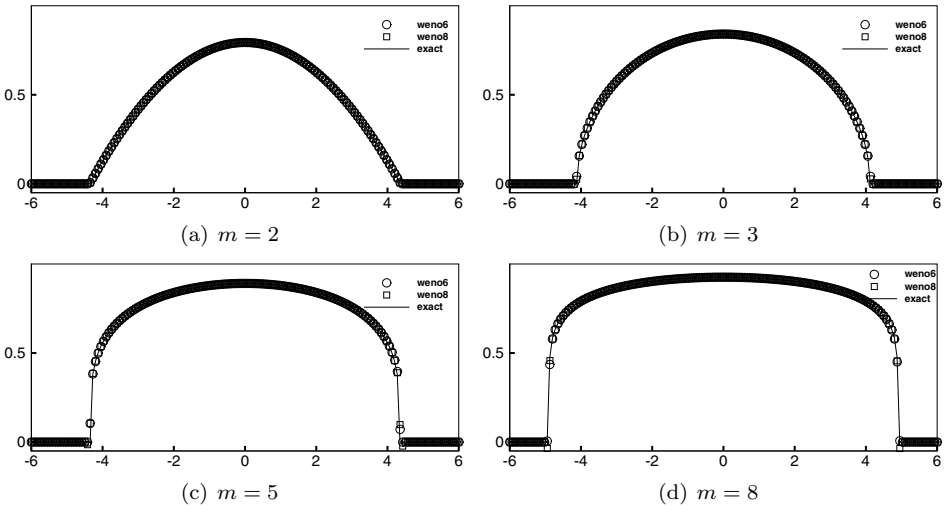

(a) $m = 2$ (b) $m = 3$

(c) $m = 5$ (d) $m = 8$

FIG. 2.1. *Barenblatt solution for the PME* (1.2). $T = 2$.

schemes produce numerical solutions accurately without noticeable oscillations for Examples 3–9; hence we present the numerical results of only the sixth order WENO scheme with $\max_u |b'(u)| \frac{\Delta t}{\Delta x^2} = 0.4$ to save space.

Example 3. We now consider the collision of the two-box solution with the same or different heights. If the variable u is regarded as the temperature, the model case is used to describe how the temperature changes when two hot spots are suddenly put in the computational domain.

In Figure 2.2, we plot the evolution of the numerical solution for the PME with $m = 5$ and the initial condition being the two-box solution with the same height:

$$u(x,0) = \begin{cases} 1 & \text{if } x \in (-3.7,-0.7) \cup (0.7,3.7), \\ 0 & \text{otherwise.} \end{cases} \tag{2.56}$$

The boundary condition is $u(\pm 5.5, t) = 0$ for $t > 0$, and the computational domain $[-5.5, 5.5]$ is divided into $N = 160$ uniform cells.

We also consider the collision of the two-box solution with different heights. Figure 2.3 is the evolution of the numerical solution for the PME with $m = 6$. The initial condition is

$$u(x,0) = \begin{cases} 1 & \text{if } x \in (-4,-1), \\ 2 & \text{if } x \in (0,3), \\ 0 & \text{otherwise.} \end{cases} \tag{2.57}$$

The boundary condition is $u(\pm 6, t) = 0$ for $t > 0$, and the computational domain is divided into $N = 160$ uniform cells.

From Figures 2.2 and 2.3, we can see that, regardless of whether the heights of the two boxes in the initial condition are the same or not, the two-box solutions first move outward independently before the collision, then they join each other to make the temperature smooth, and finally the solution becomes almost constant in the common support, agreeing with the results in [37].

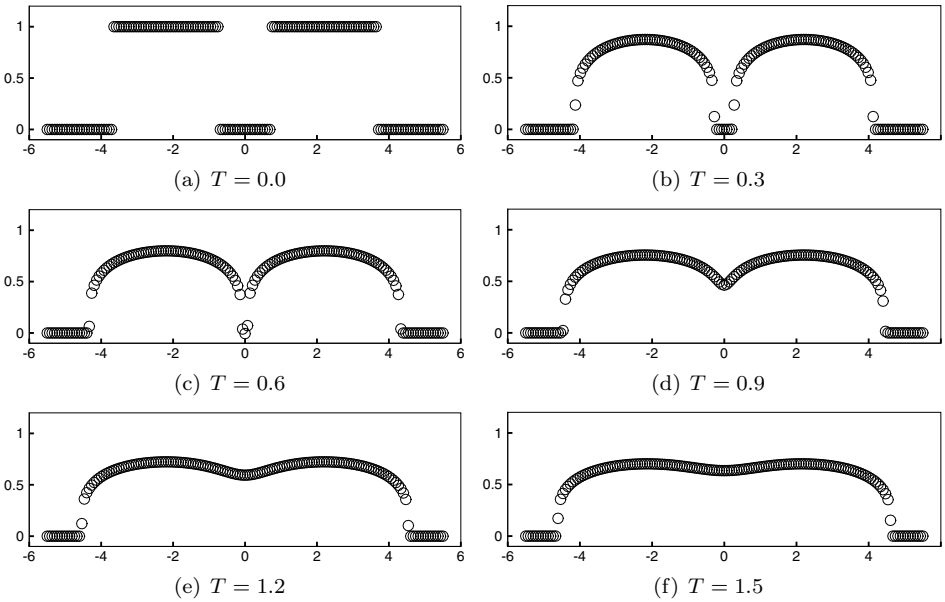

(a) $T = 0.0$ (b) $T = 0.3$ (c) $T = 0.6$ (d) $T = 0.9$ (e) $T = 1.2$ (f) $T = 1.5$

FIG. 2.2. *Collision of the two-box solution with the same height.*

Example 4. Next we consider the scalar convection-diffusion Buckley–Leverett equation

$$u_t + f(u)_x = \varepsilon(\nu(u)u_x)_x, \quad \varepsilon\nu(u) \geq 0. \tag{2.58}$$

This is a prototype model for oil reservoir simulations (two-phase flow) and is often used to test algorithms, e.g., in [20]. In our test we take $\varepsilon = 0.01$, and the flux $f(u)$ to have an s-shaped form,

$$f(u) = \frac{u^2}{u^2 + (1-u)^2}, \tag{2.59}$$

and

$$\nu(u) = \begin{cases} 4u(1-u), & 0 \leq u \leq 1, \\ 0 & \text{otherwise.} \end{cases} \tag{2.60}$$

The initial function is

$$u(x,0) = \begin{cases} 1 - 3x, & 0 \leq x \leq \frac{1}{3}, \\ 0, & \frac{1}{3} < x \leq 1, \end{cases} \tag{2.61}$$

and the boundary condition is $u(0,t) = 1$.

With the Lax–Friedrichs flux splitting, we apply the fifth order finite difference WENO scheme [17] to approximate the convection term. The numerical solution computed for different numbers of grid points is shown in Figure 2.4. The numerical results seem to converge to the correct entropy solution nicely, compared with the numerical solutions in [20].

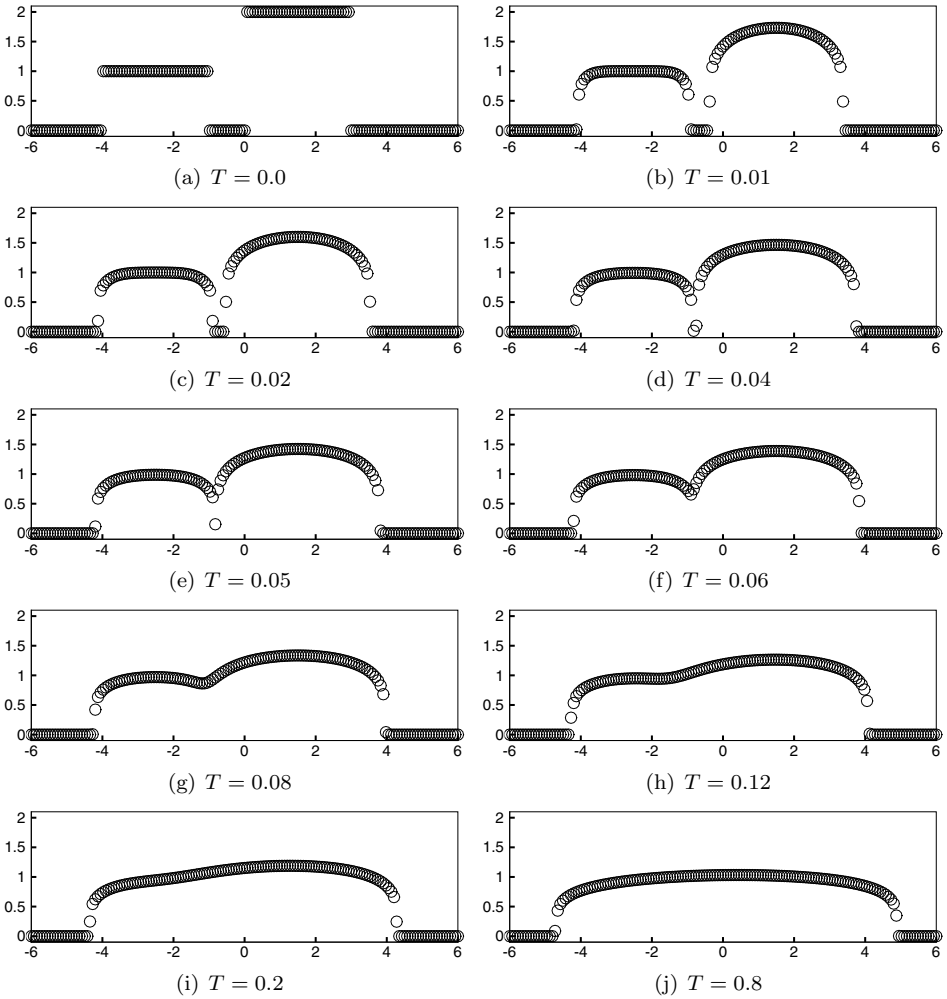

(a) $T = 0.0$ (b) $T = 0.01$

(c) $T = 0.02$ (d) $T = 0.04$

(e) $T = 0.05$ (f) $T = 0.06$

(g) $T = 0.08$ (h) $T = 0.12$

(i) $T = 0.2$ (j) $T = 0.8$

FIG. 2.3. *Collision of the two-box solution with different heights.*

Example 5. Now we consider the Buckley–Leverett equation (2.58) with $\varepsilon = 0.01$, the same diffusion coefficient (2.60), and the flux function $f(u)$ with gravitational effects:

$$f(u) = \frac{u^2}{u^2 + (1-u)^2}(1 - 5(1-u)^2). \tag{2.62}$$

We again use the fifth order finite difference WENO scheme [17] to approximate the convection term with the Lax–Friedrichs splitting. The numerical solutions to the problem (2.62) and to the problem (2.58)–(2.60) with the initial condition

$$u(x,0) = \begin{cases} 0, & 0 \le x < 1 - \frac{1}{\sqrt{2}}, \\ 1, & 1 - \frac{1}{\sqrt{2}} \le x \le 1, \end{cases}$$

are shown in Figure 2.5.

Figure 2.5 shows that the finite difference WENO scheme produces numerical solutions accurately without noticeable oscillations for both Riemann problems with

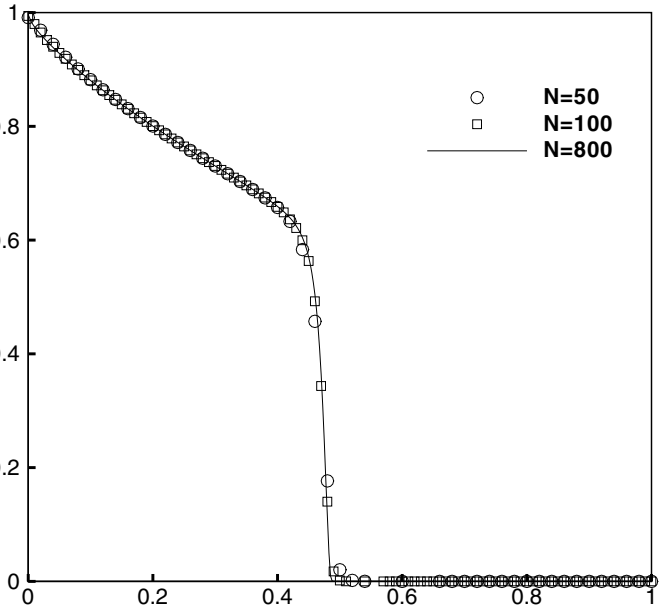

FIG. 2.4. *Initial-boundary value problem* (2.58)–(2.61). $T = 0.2$.

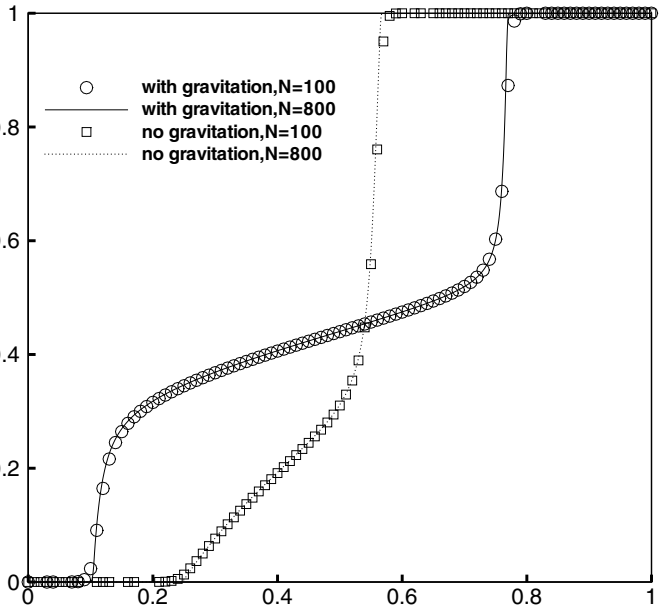

FIG. 2.5. *Riemann problem for the Buckley–Leverett equation with and without gravitation.* $T = 0.2$.

and without gravitational effects. The results compare well with those in [20].

Example 6. Next we consider a one-dimensional model for the glacier growth [14, 19]. The evolution of a glacier of height $h(x,t)$ resting upon a flat mountain can be described by the nonhomogeneous convection-diffusion equation

$$h_t + f(h)_x = \varepsilon(\nu(h)h_x)_x + S(x,t,h) \tag{2.63}$$

with $\varepsilon = 0.01$ and

$$f(h) = \frac{h+3h^6}{4}, \qquad \nu(h) = 3h^6. \tag{2.64}$$

We solve the Riemann problem with the initial data

$$h(x,0) = \begin{cases} 1, & x < 0, \\ 0, & x > 0, \end{cases}$$

which describes the outlet into a valley disregarding seasonal variations. The source term is taken as $S(x,t,h) = S_0(x)$ if $h(x,t) > 0$, and $S(x,t,h) = \max(S_0(x),0)$ if $h(x,t) = 0$, where

$$S_0(x) = \begin{cases} 0, & x < -0.4, \\ \frac{1}{2}(x+0.4), & -0.4 \le x \le -0.2, \\ -\frac{1}{2}x, & x > -0.2. \end{cases}$$

The numerical solutions are shown in Figure 2.6 for different numbers of grid points at different times. They seem to converge well with grid refinement and agree well with the results in [19, 20].

Example 7. In this test we consider an example of a strongly degenerate parabolic convection-diffusion equation presented in [20]:

$$u_t + f(u)_x = \varepsilon(\nu(u)u_x)_x, \quad \varepsilon\nu(u) \ge 0.$$

We take $\varepsilon = 0.1$, $f(u) = u^2$, and

$$\nu(u) = \begin{cases} 0, & |u| \le 0.25, \\ 1, & |u| > 0.25. \end{cases} \tag{2.65}$$

Therefore, the equation is hyperbolic when $u \in [-0.25, 0.25]$ and parabolic elsewhere. We solve the problem with the initial function

$$u(x,0) = \begin{cases} 1, & -\frac{1}{\sqrt{2}} - 0.4 < x < -\frac{1}{\sqrt{2}} + 0.4, \\ -1, & \frac{1}{\sqrt{2}} - 0.4 < x < \frac{1}{\sqrt{2}} + 0.4, \\ 0 & \text{otherwise.} \end{cases} \tag{2.66}$$

The numerical simulations for different numbers of grid points are presented in Figure 2.7 and agree well with the results in [20].

Example 8. Our finite difference WENO scheme (2.45) can also be easily extended to higher dimensions, since derivatives in each dimension can be approximated using the one-dimensional point values in that dimension. Here we present a numerical simulation for the two-dimensional PME

$$u_t = (u^2)_{xx} + (u^2)_{yy} \tag{2.67}$$

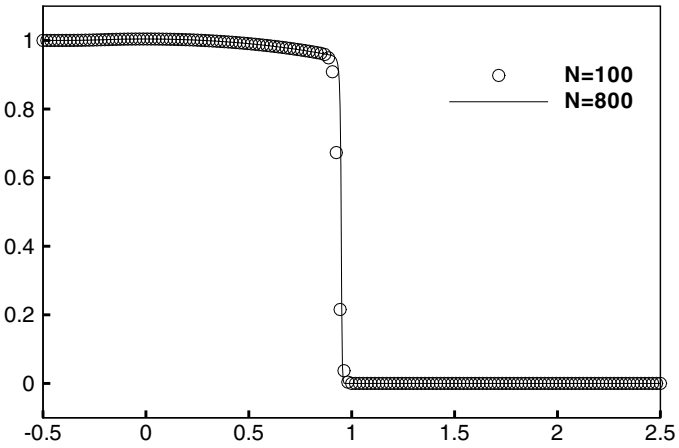

(a) $T = 1$

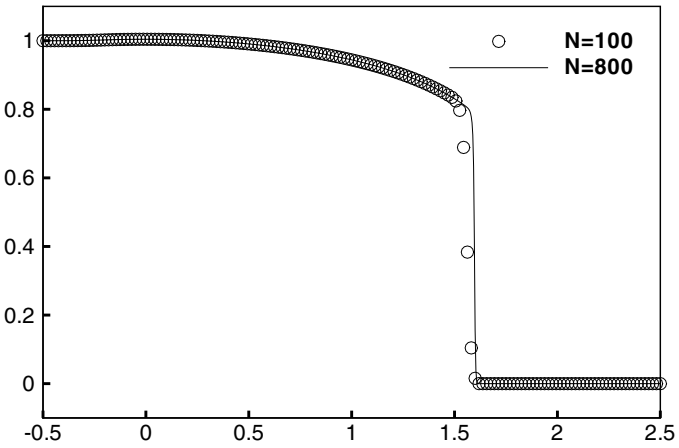

(b) $T = 2$

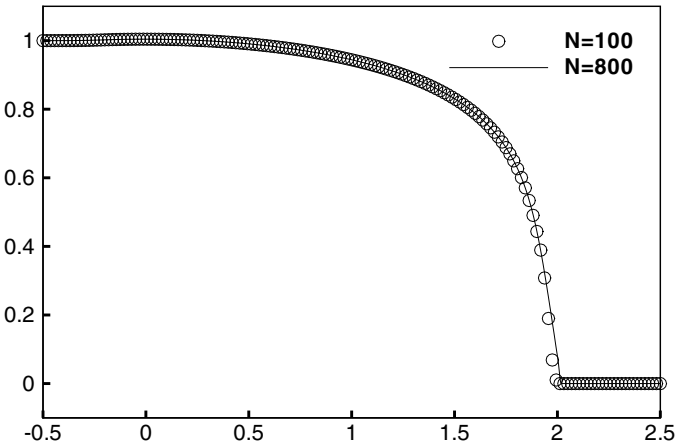

(c) $T = 4$

FIG. 2.6. *Moving glacier.*

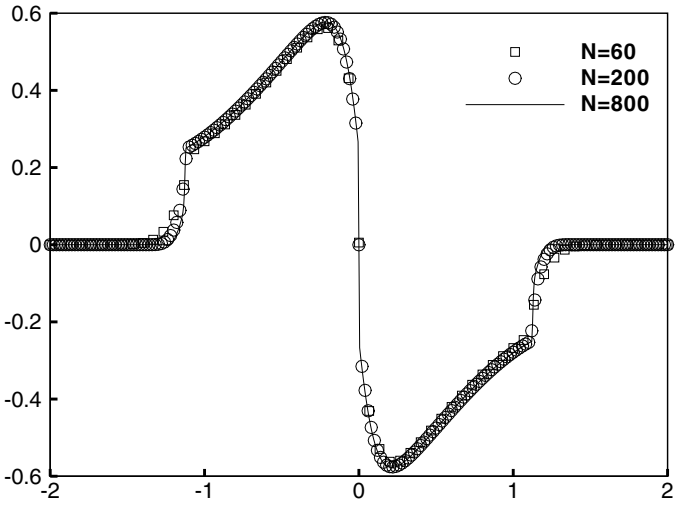

FIG. 2.7. *Riemann problem* (2.58), (2.65), *and* (2.66). $T = 0.7$.

with the initial condition $u(x, y, 0)$ given by two bumps

$$u(x,y,0) = \begin{cases} e^{\frac{-1}{6-(x-2)^2-(y+2)^2}}, & (x-2)^2+(y+2)^2 < 6, \\ e^{\frac{-1}{6-(x+2)^2-(y-2)^2}}, & (x+2)^2+(y-2)^2 < 6, \\ 0 & \text{otherwise}, \end{cases} \tag{2.68}$$

and periodic boundary conditions on $[-10, 10] \times [-10, 10]$. We compute on the large domain to ensure that the compact support of the solution can still be contained in the computational domain at the final time of the simulation. We show the numerical results at $T = 0$, 0.5, 1.0, and 4.0 in Figure 2.8 from the top left to the bottom right, respectively, with the computational domain $[-10, 10] \times [-10, 10]$ divided into 80×80 uniform cells. The results compare well with those in [8].

Example 9. Consider the two-dimensional extension of the equation in Example 7 given in [20],

$$u_t + f(u)_x + f(u)_y = \varepsilon(\nu(u)u_x)_x + \varepsilon(\nu(u)u_y)_y,$$

with $\varepsilon = 0.1$, $f(u) = u^2$, and $\nu(u)$ given in (2.65). The initial solution is

$$u(x,y,0) = \begin{cases} 1, & (x+0.5)^2+(y+0.5)^2 < 0.16, \\ -1, & (x-0.5)^2+(y-0.5)^2 < 0.16, \\ 0 & \text{otherwise}. \end{cases} \tag{2.69}$$

The numerical simulation at $T = 0.5$ is presented in Figure 2.9 with the computational domain $[-1.5, 1.5] \times [-1.5, 1.5]$ divided into 80×80 uniform cells, which compares well with that in [20].

2.6. The second formulation: Rewriting into a system. In this section we would like to briefly describe the second formulation of a WENO finite difference scheme by following the idea of the local discontinuous Galerkin method [11] to first rewrite (1.1) as a nonlinear system of first order equations

$$u_t = v_x, \tag{2.70}$$

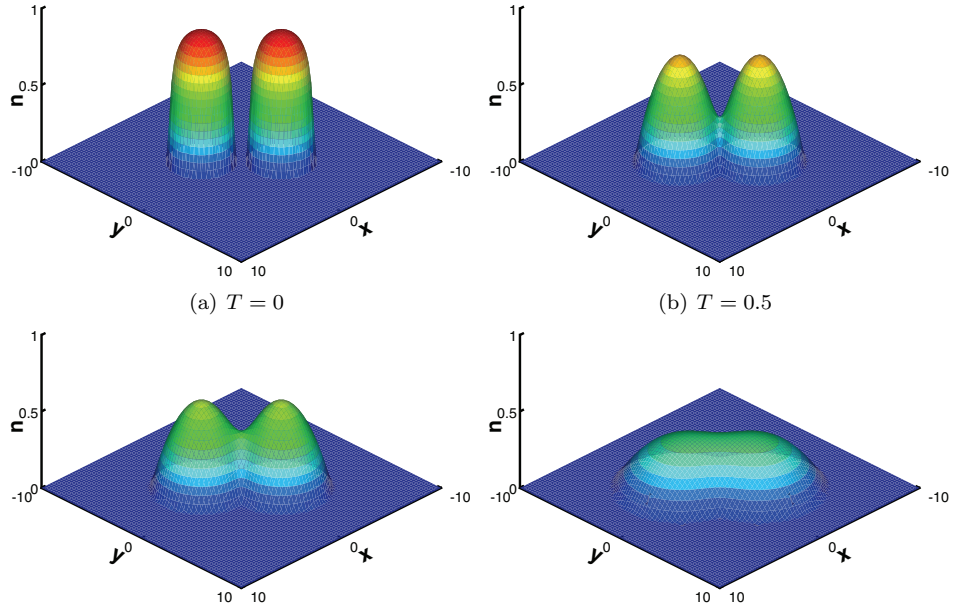

FIG. 2.8. *The numerical solution of the PME in two dimensions.*

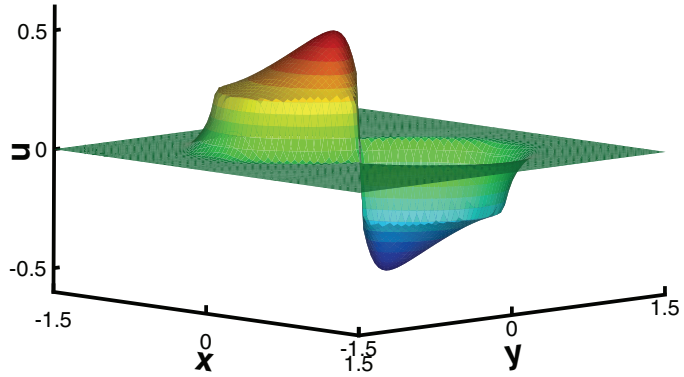

FIG. 2.9. *Degenerate parabolic problem-solution at time* $T = 0.5$ *on an* 80×80 *grid.*

$$v = b(u)_x \tag{2.71}$$

and then to solve the two first order equations, respectively, using the fifth order finite difference WENO method for conservation laws [17]. This approach has the advantage of simplicity, and it is easier to generalize it to higher than second order PDEs. However, the computational cost is larger since two WENO approximations rather than one must be used to approximate the second derivative. The effective stencil, which is a composition of two successive WENO procedures, is also wider in comparison with the first approach. To make the final effective stencil smaller, we could use a right-biased stencil for (2.70) followed by a left-biased stencil for (2.71). We have formulated and numerically tested WENO schemes in this approach. It seems that the correct order of accuracy can be obtained, but the error magnitude is

larger than that of the direct WENO method described in the previous subsections on the same mesh. For nonsmooth problems nonoscillatory results can be achieved. We omit further details here to save space.

3. Concluding remarks. In this paper we consider WENO schemes for approximating possibly degenerate parabolic equations. The formulation directly approximates the second derivative term using a conservative flux difference. The sixth order and eighth order schemes are constructed as examples. Numerical examples demonstrate that the finite difference WENO scheme can achieve high order accuracy and can simulate discontinuous solutions without oscillations.

REFERENCES

[1] H. W. Alt and S. Luckhaus, *Quasilinear elliptic-parabolic differential equations*, Math. Z., 183 (1983), pp. 311–341.
[2] D. Aregba-Driollet, R. Natalini, and S. Tang, *Explicit diffusive kinetic schemes for nonlinear degenerate parabolic systems*, Math. Comp., 73 (2004), pp. 63–94.
[3] D. G. Aronson, *The porous medium equation*, in Nonlinear Diffusion Problems, Lecture Notes in Math. 1224, Springer Berlin, 1986, pp. 1–46.
[4] D. Balsara and C.-W. Shu, *Monotonicity preserving weighted essentially non-oscillatory schemes with increasingly high order of accuracy*, J. Comput. Phys., 160 (2000), pp. 405–452.
[5] G. I. Barenblatt, *On self-similar motions of compressible fluid in a porous medium*, Prikl. Mat. Mekh., 16 (1952), pp. 679–698 (in Russian).
[6] A. E. Berger, H. Brezis, and J. C. Rogers, *A numerical method for solving the problem* $u_t - \Delta f(u) = 0$, RAIRO Anal. Numér., 13 (1979), pp. 297–312.
[7] E. Carlini, R. Ferretti, and G. Russo, *A weighted essentially nonoscillatory, large time-step scheme for Hamilton-Jacobi equations*, SIAM J. Sci. Comput., 27 (2005), pp. 1071–1091.
[8] F. Cavalli, G. Naldi, G. Puppo, and M. Semplice, *High-order relaxation schemes for nonlinear degenerate diffusion problems*, SIAM J. Numer. Anal., 45 (2007), pp. 2098–2119.
[9] C.-S. Chou and C.-W. Shu, *High order residual distribution conservative finite difference WENO schemes for steady state problems on non-smooth meshes*, J. Comput. Phys., 214 (2006), pp. 698–724.
[10] C.-S. Chou and C.-W. Shu, *High order residual distribution conservative finite difference WENO schemes for convection-diffusion steady state problems on non-smooth meshes*, J. Comput. Phys., 224 (2007), pp. 992–1020.
[11] B. Cockburn and C.-W. Shu, *The local discontinuous Galerkin method for time-dependent convection-diffusion systems*, SIAM J. Numer. Anal., 35 (1998), pp. 2440–2463.
[12] C. J. van Duyn and L. A. Peletier, *Nonstationary filtration in partially saturated porous media*, Arch. Ration. Mech. Anal., 78 (1982), pp. 173–198.
[13] S. Evje and K. H. Karlsen, *Viscous splitting approximation of mixed hyperbolic-parabolic convection-diffusion equations*, Numer. Math., 83 (1999), pp. 107–137.
[14] A. C. Flower, *Glaciers and ice sheets*, in The Mathematics of Model for Climatology and Environment, J. I. Diaz, ed., NATO ASI Series, Springer-Verlag, Berlin, 48 (1996), pp. 302–336.
[15] A. K. Henrick, T. D. Aslam, and J. M. Powers, *Mapped weighted essentially non-oscillatory schemes: Achieving optimal order near critical points*, J. Comput. Phys., 207 (2005), pp. 542–567.
[16] W. Jäger and J. Kačur, *Solution of porous medium type systems by linear approximation schemes*, Numer. Math., 60 (1991), pp. 407–427.
[17] G. Jiang and C.-W. Shu, *Efficient implementation of weighted ENO schemes*, J. Comput. Phys., 126 (1996), pp. 202–228.
[18] J. Kačur, A. Handlovičová, and M. Kačurová, *Solution of nonlinear diffusion problems by linear approximation schemes*, SIAM J. Numer. Anal., 30 (1993), pp. 1703–1722.
[19] K. H. Karlsen and K. A. Lie, *An unconditionally stable splitting for a class of nonlinear parabolic equations*, IMA J. Numer. Anal., 19 (1999), pp. 609–635.
[20] A. Kurganov and E. Tadmor, *New high-resolution central schemes for nonlinear conservation laws and convection-diffusion equations*, J. Comput. Phys., 160 (2000), pp. 241–282.
[21] X.-D. Liu, S. Osher, and T. Chan, *Weighted essentially non-oscillatory schemes*, J. Comput. Phys., 115 (1994), pp. 200–212.

[22] Y. Liu, C.-W. Shu, and M. Zhang, *On the positivity of linear weights in WENO approximations*, Acta Math. Appl. Sin. Engl. Ser., 25 (2009), pp. 503–538.
[23] Y. Lu and W. Jäger, *On solutions to nonlinear reaction-diffusion-convection equations with degenerate diffusion*, J. Differential Equations, 170 (2001), pp. 1–21.
[24] E. Magenes, R. H. Nochetto, and C. Verdi, *Energy error estimates for a linear scheme to approximate nonlinear parabolic problems*, RAIRO Math. Model. Numer. Anal., 21 (1987), pp. 655–678.
[25] B. Merryman, *Understanding the Shu-Osher conservative finite difference form*, J. Sci. Comput., 19 (2003), pp. 309–322.
[26] M. Muskat, *The Flow of Homogeneous Fluids Through Porous Media*, McGraw-Hill, New York, 1937.
[27] R. H. Nochetto, A. Schmidt, and C. Verdi, *A posteriori error estimation and adaptivity for degenerate parabolic problems*, Math. Comp., 69 (2000), pp. 1–24.
[28] R. H. Nochetto and C. Verdi, *Approximation of degenerate parabolic problems using numerical integration*, SIAM J. Numer. Anal., 25 (1988), pp. 784–814.
[29] F. Otto, *L1-contraction and uniqueness for quasilinear elliptic-parabolic equations*, J. Differential Equations, 131 (1996), pp. 20–38.
[30] I. S. Pop and W. Yong, *A numerical approach to degenerate parabolic equations*, Numer. Math., 92 (2002), pp. 357–381.
[31] K. Sebastian and C.-W. Shu, *Multi domain WENO finite difference method with interpolation at sub-domain interfaces*, J. Sci. Comput., 19 (2003), pp. 405–438.
[32] J. Shi, C. Hu, and C.-W. Shu, *A technique of treating negative weights in WENO schemes*, J. Comput. Phys., 175 (2002), pp. 108–127.
[33] C.-W. Shu, *Essentially non-oscillatory and weighted essentially non-oscillatory schemes for hyperbolic conservation laws*, in Advanced Numerical Approximation of Nonlinear Hyperbolic Equations, Lecture Notes in Math. 1697, Springer, Berlin, 1998, pp. 325–432.
[34] C.-W. Shu, *High order weighted essentially non-oscillatory schemes for convection dominated problems*, SIAM Rev., 51 (2009), pp. 82–126.
[35] C.-W. Shu and S. Osher, *Efficient implementation of essentially non-oscillatory shock-capturing schemes*, J. Comput. Phys., 77 (1988), pp. 439–471.
[36] Ya. B. Zel'dovich and A. S. Kompaneetz, *Towards a theory of heat conduction with thermal conductivity depending on the temperature*, in Collection of Papers Dedicated to the 70th Anniversary of A. F. Ioffe, Izd. Akad. Nauk SSSR, Moscow, 1950, pp. 61–72.
[37] Q. Zhang and Z. Wu, *Numerical simulation for porous medium equation by local discontinuous Galerkin finite element method*, J. Sci. Comput., 38 (2009), pp. 127–148.